SANDIA REPORT

SAND2010-6571
Unlimited Release
Printed October 2010

Fluorescence Measurements for Evaluating the Application of Multivariate Analysis Techniques to Optically Thick Environments

Thomas A. Reichardt, Randal L. Schmitt, Shane M. Sickafoose, Howland D. T. Jones, and Jerilyn A. Timlin

Prepared by
Sandia National Laboratories
Albuquerque, New Mexico 87185 and Livermore, California 94550

Sandia National Laboratories is a multi-program laboratory managed and operated by Sandia Corporation, a wholly owned subsidiary of Lockheed Martin Corporation, for the U.S. Department of Energy's National Nuclear Security Administration under contract DE-AC04-94AL85000.

Issued by Sandia National Laboratories, operated for the United States Department of Energy by Sandia Corporation.

Available to DOE and DOE contractors from
U.S. Department of Energy
Office of Scientific and Technical Information
P.O. Box 62
Oak Ridge, TN 37831

Telephone: (865)576-8401
Facsimile: (865)576-5728
E-Mail: reports@adonis.osti.gov
Online ordering: http://www.osti.gov/bridge

Available to the public from
U.S. Department of Commerce
National Technical Information Service
5285 Port Royal Rd
Springfield, VA 22161

Telephone: (800)553-6847
Facsimile: (703)605-6900
E-Mail: orders@ntis.fedworld.gov
Online order: http://www.ntis.gov/help/ordermethods.asp?loc=7-4-0#online

SAND2010-6571
Unlimited Release
Printed October 2010

Fluorescence Measurements for Evaluating the Application of Multivariate Analysis Techniques to Optically Thick Environments

Thomas A. Reichardt
Remote Sensing and Energetic Materials
Sandia National Laboratories
PO Box 969, MS 9056
Livermore, California 94551-0956

Randal L. Schmitt and Shane M. Sickafoose
Lasers, Optics, and Remote Sensing
Sandia National Laboratories
PO Box 5800, MS 1423
Albuquerque, New Mexico 87185-1423

Howland D. T. Jones and Jerilyn A. Timlin
Bioenergy and Defense Technology
Sandia National Laboratories
PO Box 5800, MS 0895
Albuquerque, New Mexico 87185-0895

Abstract

Laser-induced fluorescence measurements of cuvette-contained laser dye mixtures are made for evaluation of multivariate analysis techniques to optically thick environments. Nine mixtures of Coumarin 500 and Rhodamine 610 are analyzed, as well as the pure dyes. For each sample, the cuvette is positioned on a two-axis translation stage to allow the interrogation at different spatial locations, allowing the examination of both primary (absorption of the laser light) and secondary (absorption of the fluorescence) inner filter effects. In addition to these expected inner filter effects, we find evidence that a portion of the absorbed fluorescence is re-emitted. A total of 688 spectra are acquired for the evaluation of multivariate analysis approaches to account for nonlinear effects.

CONTENTS

1. Introduction 7
2. Experiment 9
2.1. Laser Excitation and Optical Detection 9
2.2. Positioning the Cuvettes 10
2.3. Dye Mixtures 11
3. Acquired Spectra: Evidence of Fluorescence Re-Emission 13
4. Summary 17
References 21

Figures

Fig. 1. Geometry for spatially resolved laser-induced fluorescence measurments on cuvette-contained samples. The origin is positioned 0.5 mm from the inner surface of the cuvette windows. 9

Fig. 2. Relative gain provided by the ICCD as a function of the gain setting referenced to a gain setting of 0. These measurements were performed on quinine water. 10

Fig. 3. ICCD full-frame images for x = 1.0 mm, y = 0.0 to 7.0 mm. The system is configured fo optimal focusing at y = 4.0 mm. Due to the wavelength-dependent index of refraction of methanol, the shorter wavelenth range is less sharply focused than the longer wavelength range for y = 0.0 mm (top), while the reverse is true for y = 7.0 mm (bottom). 11

Fig. 4. Absorbance measurements performed with a Cary 500 spectrophotometer on 10x diluted samples of the pure Coumarin and Rhodamine dye mixtures. The absorbance is normalized to the concentration (mg/L) of each dye to allow comparison of these measurements to results in the literature. 12

Fig. 5. Flourescence measurements at different (*x*,*y*) locations for 100% Coumarin..... 14

Fig. 6. Flourescence measurements at different (*x*,*y*) locations for 90% Coumarin, 10% Rhodamine. 14

Fig. 7. Flourescence measurements at different (*x*,*y*) locations for 80% Coumarin, 20% Rhodamine. 14

Fig. 8. Flourescence measurements at different (*x*,*y*) locations for 70% Coumarin, 30% Rhodamine. 14

Fig. 9. Flourescence measurements at different (*x*,*y*) locations for 60% Coumarin, 40% Rhodamine. 15

Fig. 10. Flourescence measurements at different (*x*,*y*) locations for 50% Comarin, 50% Rhodamine. 15

Fig. 11. Flourescence measurements at different (*x*,*y*) locations for 40% Coumarin, 60% Rhodamine. 15

Fig. 12. Flourescence measurements at different (*x*,*y*) locations for 30% Coumarin, 70% Rhodamine. 15

Fig. 13. Flourescence measurements at different (*x*,*y*) locations for 20% Coumarin, 80% Rhodamine. 16

Fig. 14. Flourescence measurements at different (*x*,*y*) locations for 10% Comarin, 90% Rhodamine. 16

Fig. 15. Flourescence measurements at different (*x*,*y*) locations for 100% Rhodamine. 16

Fig. 16. Absorbance for a 50/50 mixture of the Coumarin and Rhodamine dyes calculated by applying Eq. (1) to the data displayed in Fig. 10.. 17

1. Introduction

Fluorescence excitation-emission data are utilized in the fields of medicine [1] and analytical chemistry [2], as well as for scientific studies focused on the environment [3], defense/security [4], and energy [5]. Specifically relating to energy research, Sandia has recently begun an effort to characterize the fluorescence signatures of bulk algal samples for assessment of both local and remote approaches for appraisal of algal health for biofuel production [6]. Considering a matrix of excitation-emission data, the norm of the matrix is ideally proportional to the outer product of the excitation spectrum and emission spectrum [7]. However, nonlinear deviations, also known as inner filter effects, can result from absorption of both the excitation (termed "primary absorption") and fluorescence (termed "secondary absorption"), with both effects increasing with increasing concentration. We note that several other factors might result in a departure from this simple linear model, including diffusion, temperature and pH variations, fluorescence quenching, and ionic strength [8], but we limit this study to inner filter effects.

Adamsons et al. [9] summarize previous work evaluating inner filter effects, and we present a condensed version of their review here. In 1938, Sen-Gupta [10] presented the first theoretically derived expressions accounting for inner filter effects in the right angle geometry for a single fluorophore. Further studies followed pertaining to multiple fluorophores, and more in-depth mathematical studies were applied to the problem in the 1950s [11,12], with additional treatment of the measurement geometry occurring in the 1960s [13,14]. In 1973, Van Slageren et al. [15] published a theoretical account that included cell geometry, primary and secondary absorptions, and cell surface reflections. In the 1970's and 1980's it was recognized that using a vibrating mirror [16,17], or shifting [18] or rotating [9,19] the cell could account for inner filter effects. Improvement of these methods, such as automating the cuvette translation [20-22], continued with Tucker et al. publishing a related tutorial article [23] in 1992. Accounting for inner filter effects with alternative methods, such as Raman scattering [24], continue.

In this work, we acquire a dataset to perform an evaluation of multivariate approaches to account for inner filter effects. In addition to primary and secondary absorption, we see evidence that a significant fraction of the absorbed fluorescence is re-emitted. We anticipate that such effects will be important when probing algal samples, for which the absorption and emission spectra of different pigments significantly overlap. Sandia is a recognized leader in developing and applying multivariate approaches, using such techniques to quantify the relative components in time-of-flight secondary ion mass spectrometry (TOF-SIMS), attenuated total reflectance Fourier transform infrared spectroscopy (ATR-FTIR), Raman spectroscopy, X-ray diffraction, and spectrally resolved laser-induced fluorescence (LIF). Applying multivariate approaches to data collected from the cuvette-contained samples will allow extrapolation of the cuvette results to a fieldable lidar system. More generally, the methods discussed here could have much broader applications in the field of remote sensing, where nonlinear effects routinely degrade the fidelity of analysis by linear spectral unmixing. A discussion of these potential applications is included in the summary.

2. Experiment

2.1. Laser Excitation and Optical Detection

The experimental apparatus used for these measurements is a mini-lidar system originally constructed for the analysis of cuvette-contained samples of algae. The laser source is a Sandia-built diode-pumped Nd:YAG microlaser, similar to those described by Aniolek et al. [25] and Reichardt et al. [26], frequency tripled to generate 355-nm pulses at a 100-Hz repetition rate. The laser is softly focused into the cuvette to a beam waist w of 160 µm. The cuvette is mounted on a two-axis translation stage to allow repeatable probing at different spatial locations. Figure 1 displays the coordinate system describing the location in the cuvette, where the x-coordinate corresponds to increased primary absorption of the laser beam, and the y-coordinate corresponds to increased secondary absorption of the fluorescence, as well as potential re-emission of that absorbed fluorescence. The emission is collected and collimated with a 25.4-mm diameter, 50.8-mm focal length (f#/2) achromatic lens, and the light is transmitted through a custom 355-nm blocking filter (Barr Associates), and focused onto the 100-µm vertical slit of a JY CP140-1602 f#/2 imaging spectrograph (blazed for 350 nm) with a lens identical to the collection optic, providing 1x magnification. The probe volume can therefore be considered to be a cylinder of 100-µm length (defined by the slit width) with diameter $2w$ = 320 µm.

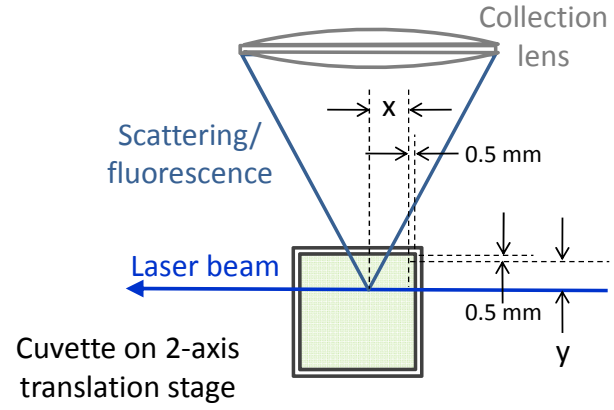

Fig. 1. Geometry for spatially resolved laser-induced fluorescence measurments on cuvette-contained samples. The origin is positioned 0.5 mm from the inner surface of the cuvette windows.

An Andor DH501-25F-913 ICCD (intensified charge-coupled device) is mounted to the spectrometer to capture the dispersed fluorescence. Unless otherwise stated, the ICCD collects data while implementing full vertical binning and with a gain setting of 50, which provides a gain of 5.6 when referenced to the gain setting of 0 (see Fig. 2), and 100 single-shot spectra are accumulated for each acquired spectrum. The horizontal pixel range of the ICCD, spectrally calibrated with a mercury lamp and a multi-wavelength HeNe laser, spans from 284 nm to 726 nm. Because any analysis of these data would likely be performed on raw ICCD counts, we present spectra in this report in terms of these counts. However, the spectrally dependent sensitivity was previously calibrated with a standard lamp, so relative temporally-integrated radiance values could be calculated from the spectra presented in this report.

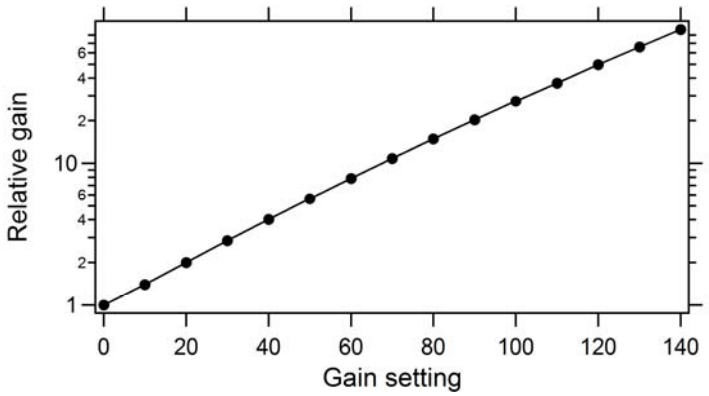

Fig. 2. Relative gain provided by the ICCD as a function of the gain setting referenced to a gain setting of 0. These measurements were performed on quinine water.

Comparing signal levels from different samples requires maintaining constant laser pulse energy. The average pulse energy is maintained at 160 +/- 2 μJ, and is monitored at ~10 minute intervals. Rotating the waveplate can account for any long term drifts, but the pulse energy is quite stable, and such waveplate adjustments are required only after several hours of operation. While the long-term stability of the laser is ~1%, the statistics output of the Coherent energy meter indicates that the laser source exhibits pulse-to-pulse energy fluctuations of +/- 7%. This measured instability warrants further investigation, because visible inspection of single-shot fluorescence data indicates that the laser is more stable than this. Nevertheless, the potential impact of these energy fluctuations is reduced by accumulating 100 laser shots for each acquired spectrum.

2.2. Positioning the Cuvettes

Quantitatively comparing spectra from different cuvette-contained samples requires consistent positioning of the cuvettes from one sample to the next. Also, decoupling the *x* and *y* translations requires that the beam path be oriented 90^{o} relative to the centerline of the detection optics. Achieving these goals requires special attention be given to the experimental configuration. Using commercial optical mounts, a cuvette mounting assembly was constructed with three contact points for repeatable cuvette positioning. Before beginning a series of measurements, we direct the laser beam path at 90^{o} with respect to the centerline of the detection optics. We then position the cuvette in the mounting assembly so the beam path is parallel to the front exit face of the cuvette. This alignment is performed by visible inspection, and a cuvette filled with quinine water typically used in this procedure. After the optics are positioned, no further alignment modifications are made for the duration of the experiment.

Ideally, the focus of the collection optics should be well-matched to the laser beam path. However, translating the cuvette in the *y*-dimension affects the focus of the collection optics due to the different indices of refraction of air and methanol, the solvent used in these experiments. Knowing that the *y*-coordinate affects the focus of the collection optics, we optimize the collection at $y = 4$ mm, approximately the midway point of *y*-translation. Figure 3 displays the full-frame spectrometer images as a function of *y*, demonstrating the sharpest focus at $y = 4.0$ mm.

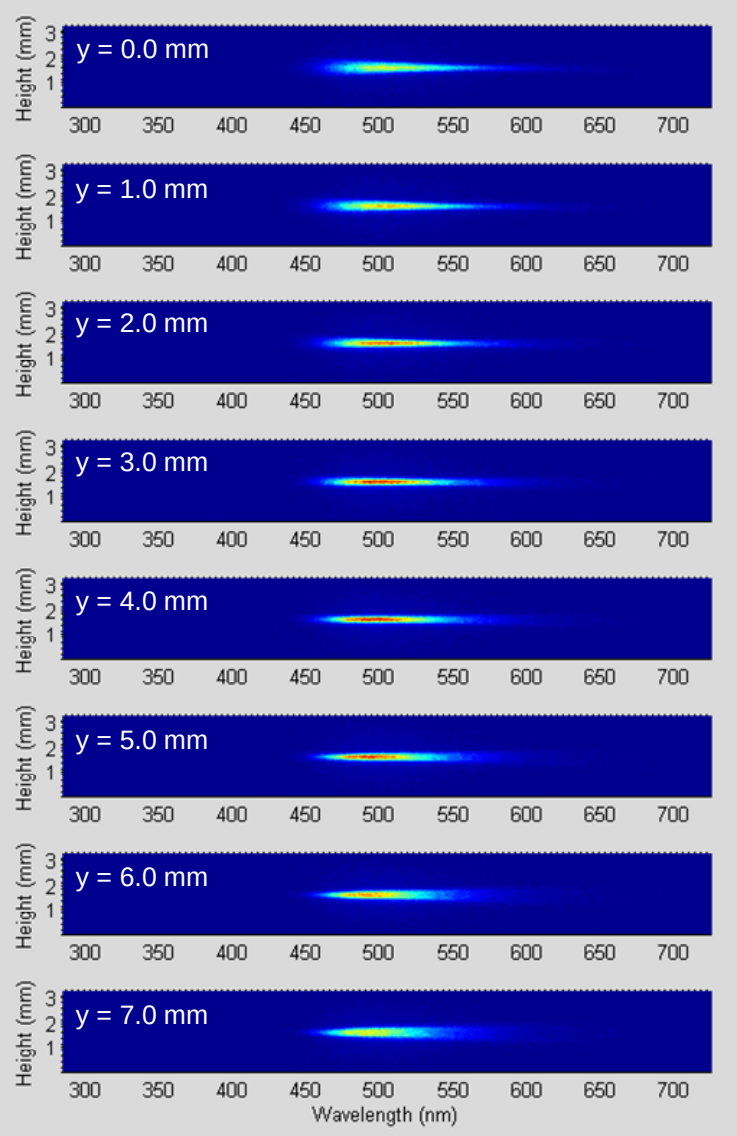

Fig. 3. ICCD full-frame images for x = 1.0 mm, y = 0.0 to 7.0 mm. The system is configured fo optimal focusing at y = 4.0 mm. Due to the wavelength-dependent index of refraction of methanol, the shorter wavelenth range is less sharply focused than the longer wavelength range for y = 0.0 mm (top), while the reverse is true for y = 7.0 mm (bottom).

The spatial coordinates of the location probed in the cuvettes is referenced to the point x = 0.0 mm, y = 0.0 mm, a position where both primary and secondary absorptions are minimized. To allow collection of data at this reference point while avoiding interference from the cuvette windows, this position is set approximately 0.5 mm from each cuvette window (see Fig. 1).

2.3. Dye Mixtures

The laser dyes Coumarin 500 and Rhodamine 610 are used in the series of measurements. These two dyes were chosen knowing that Coumarin 500 would be excited by the 355-nm light and that the resulting fluorescence from Coumarin 500 would be absorbed by the Rhodamine 610. Rhodamine 610 also absorbs 355-nm light, but to a lesser extent than Coumarin 500 does for comparable concentrations (see Fig. 4). Also, unlike Coumarin 500, the absorption and emission spectra for Rhodamine 610 significantly overlap. Mixing these two dyes in different ratios allows spanning a large range of primary and secondary absorption for a data set rich in inner filter effects. Through iterative dilutions of the two dyes, we chose concentrations for the pure dyes that resulted in similar

levels of fluorescence while providing significant attenuation of the laser excitation wavelength: the concentration of the pure Coumarin 500 is 80 mg/L, while that of the pure Rhodamine 610 is 72 mg/L.

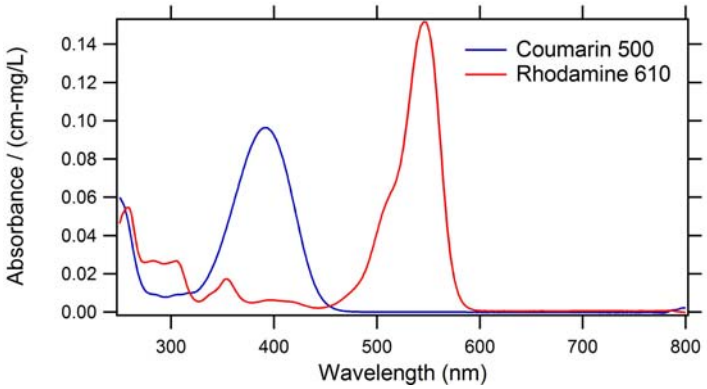

Fig. 4. Absorbance measurements performed with a Cary 500 spectrophotometer on 10x diluted samples of the pure Coumarin and Rhodamine dye mixtures. The absorbance is normalized to the concentration (mg/L) of each dye to allow comparison of these measurements to results in the literature.

3. Acquired Spectra: Evidence of Fluorescence Re-Emission

The acquired spectra span the spatial range x = 0.0-7.0 mm, y = 0.0-7.0 mm, with a 1.0-mm grid spacing. For all but x = 0.0 mm, the value of y spans the entire 7.0-mm range; for x = 0.0 mm, only y = 0.0 and 1.0 mm are analyzed, because for larger values of y the laser entry window could potentially interfere with the light path to the detector. The total 688 acquired spectra are displayed in Figs. 5-15. The figures are grouped by dye mixture, and each figure contains eight graphs, one for each value of x.

Viewing the raw data in Figs. 5-15, several initial observations can be made:

1. The variation of measured spectra with the y-coordinate is a result of self-absorption. The 460-600 nm wavelength range associated with this variation matches the primary absorption feature of Rhodamine (see Fig. 4).
2. For each value of x, the spectrum for pure Coumarin (see Fig. 5) is independent of the y-coordinate, demonstrating that Coumarin does not exhibit self-absorption. In contrast, the opposite is true for pure Rhodamine (see Fig. 15).
3. Observing Fig. 5 and comparing the graphs for x = 0.0 mm and x = 7.0 mm, we conclude that the fluorescence spectra were recorded with adequate signal-to-noise ratio even while spanning two orders of magnitude in signal strength. We anticipate that the absorption of 355-nm light could likely be calculated from the spectrally integrated signal strength as a function of x for a given value of y.

As suggested in the Introduction, fluorescence lidar measurements might be subject not only to the absorption of the initial fluorescence, but to the re-emission of that absorbed light as well. We have evidence that such re-emission is present in our laser-dye data. Figure 16 displays the calculated absorbance per cm measured as a function of y for a 50/50 mixture of the Coumarin and Rhodamine dyes. For each value of the x-coordinate, the spectrally resolved absorbance $Abs(\lambda)$ can be calculated by ratioing the spectra S_y, acquired at different y locations, to the spectrum S_0, acquired at y = 0.0 mm, through the equation

$$Abs(\lambda) = -(1/y) \times \log_{10} [\, S_y(\lambda) / S_0(\lambda) \,]. \qquad (1)$$

For all values of x, the absorbance spectrum for y = 1.0 mm agrees quite well with the spectral shape of Rhodamine absorbance measured with the Cary 500 spectrophotometer (see Fig. 4). However, for larger values of y the deviation from this reference spectrum over the 530-570 nm range is significant. Such behavior would not be expected if absorption of the initial emission were the sole secondary filtering effect. It is apparent that the 530-570 nm absorbance decreases with increasing values of y, resulting from photons absorbed at shorter wavelengths being subsequently emitted at longer wavelengths – an effect which becomes more pronounced with increasing path length of the emission through the sample.

As a consistency check, we compare the absolute absorbance values calculated for y = 1.0 mm with the spectrophotometer measurements displayed in Fig. 4. For the 50/50 mixture, the Rhodamine concentration is 0.5 × 72 mg/L = 36 mg/L, and from Fig. 4 we calculate a peak absorbance of 36 × 0.15 = 5.4. While in reasonable agreement with the peak absorbance value of ~6.5 (see Fig. 16), this 20% difference likely warrants further investigation.

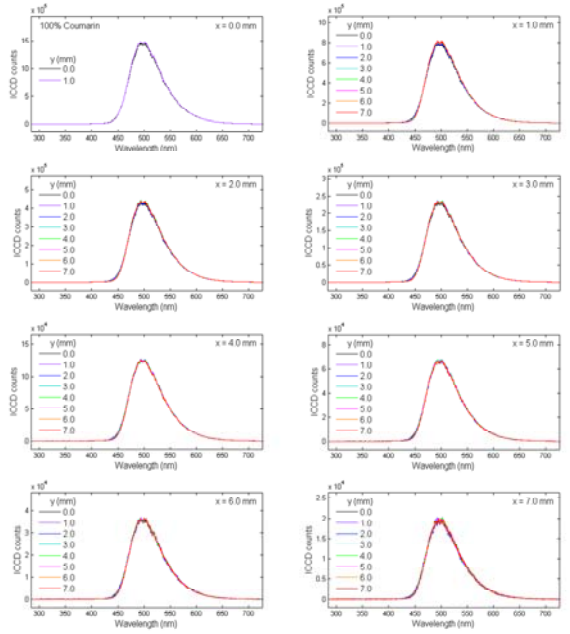

Fig. 5. Flourescence measurements at different (*x*,*y*) locations for 100% Coumarin.

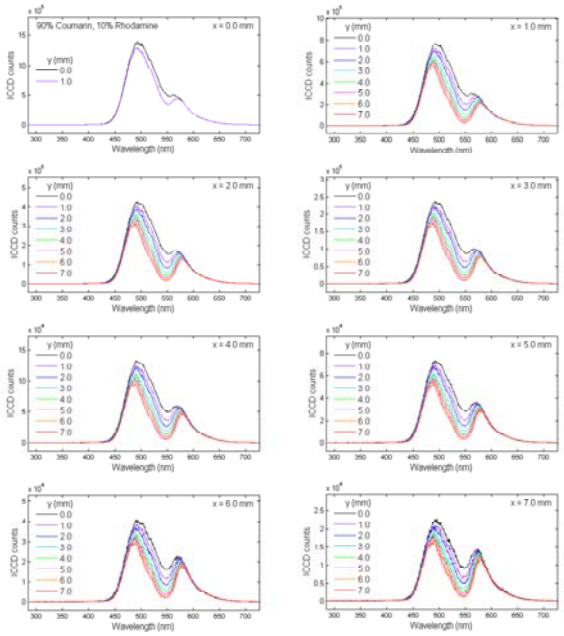

Fig. 6. Flourescence measurements at different (*x*,*y*) locations for 90% Coumarin, 10% Rhodamine.

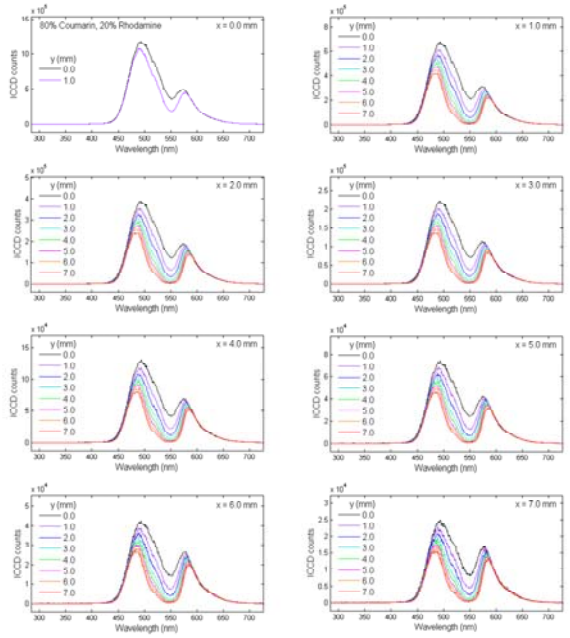

Fig. 7. Flourescence measurements at different (*x*,*y*) locations for 80% Coumarin, 20% Rhodamine.

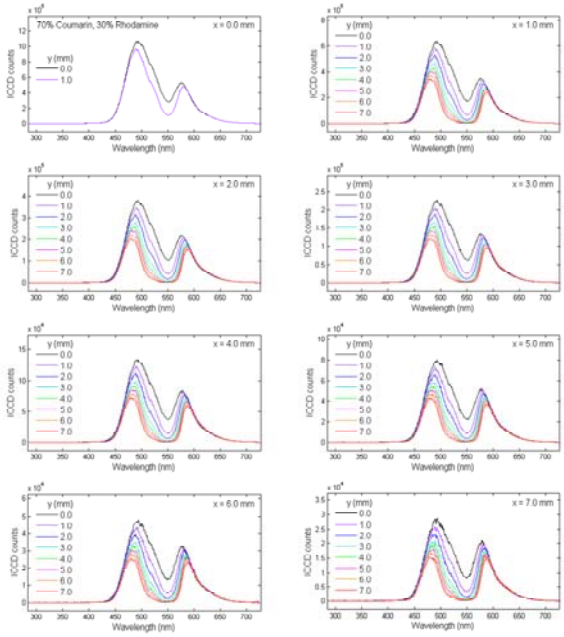

Fig. 8. Flourescence measurements at different (*x*,*y*) locations for 70% Coumarin, 30% Rhodamine.

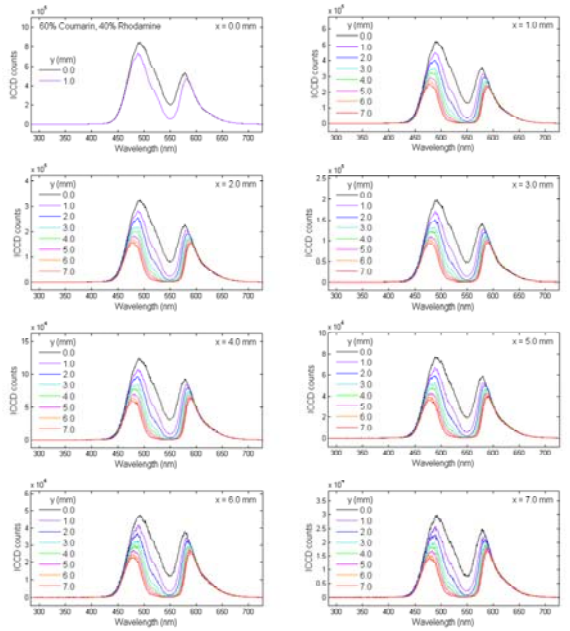

Fig. 9. Flourescence measurements at different (*x*,*y*) locations for 60% Coumarin, 40% Rhodamine.

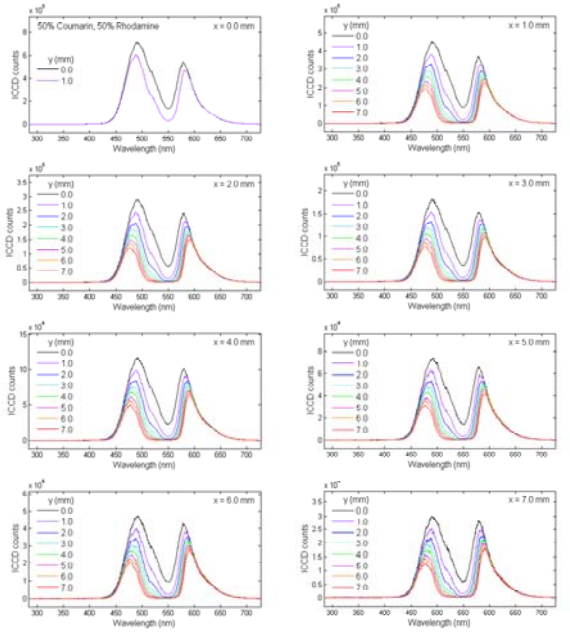

Fig. 10. Flourescence measurements at different (*x*,*y*) locations for 50% Comarin, 50% Rhodamine.

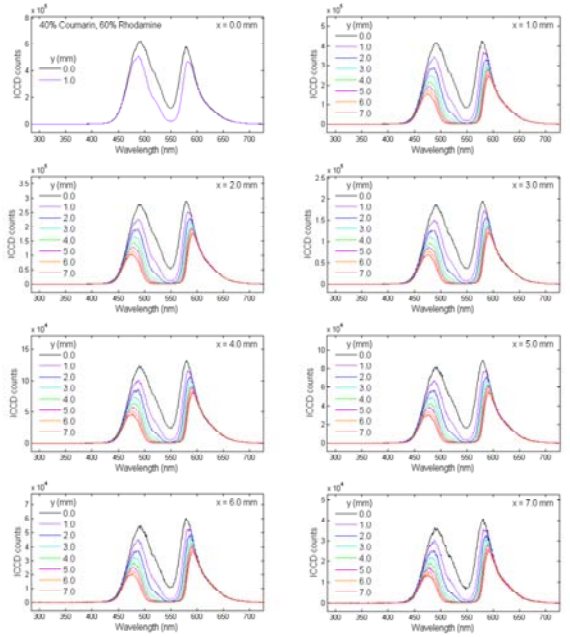

Fig. 11. Flourescence measurements at different (*x*,*y*) locations for 40% Coumarin, 60% Rhodamine.

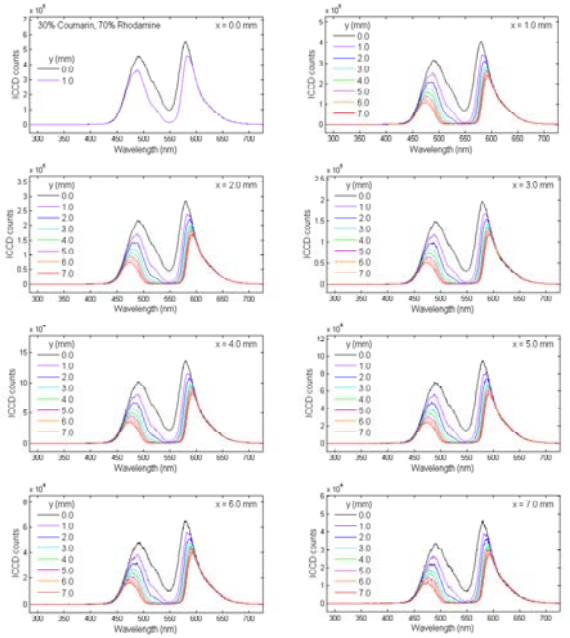

Fig. 12. Flourescence measurements at different (*x*,*y*) locations for 30% Coumarin, 70% Rhodamine.

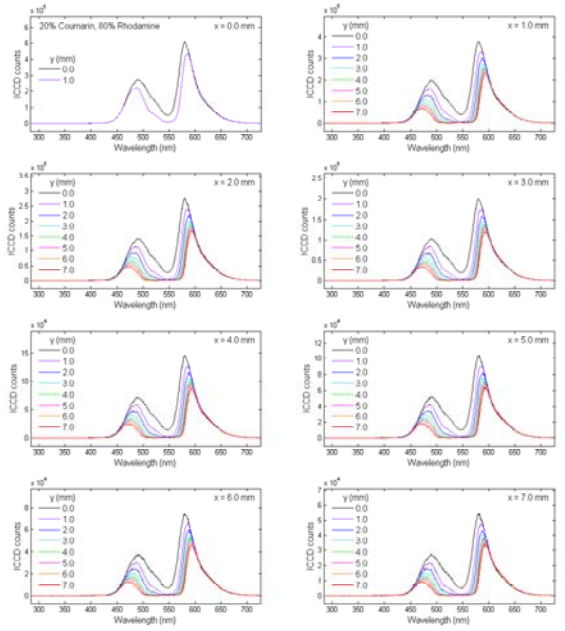

Fig. 13. Flourescence measurements at different (*x*,*y*) locations for 20% Coumarin, 80% Rhodamine.

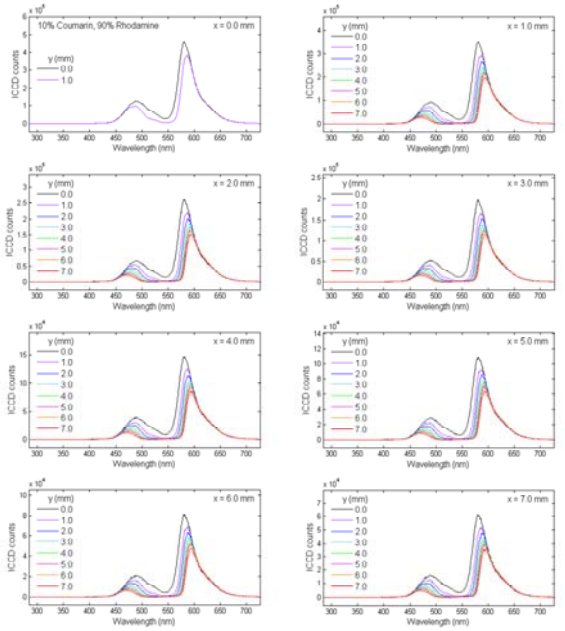

Fig. 14. Flourescence measurements at different (*x*,*y*) locations for 10% Comarin, 90% Rhodamine.

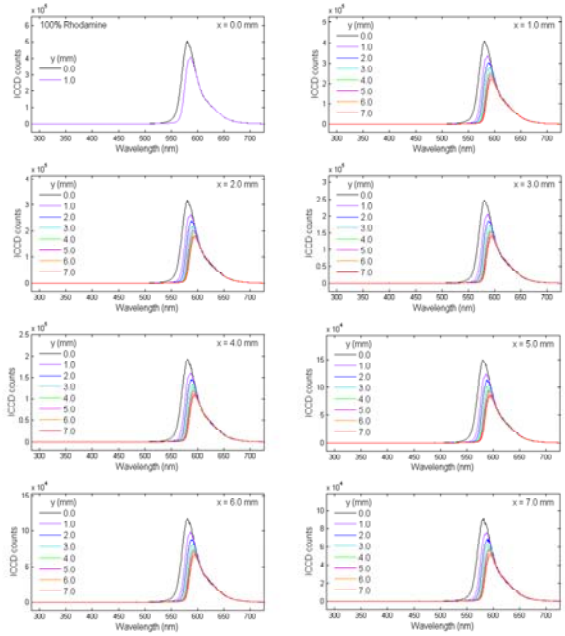

Fig. 15. Flourescence measurements at different (*x*,*y*) locations for 100% Rhodamine.

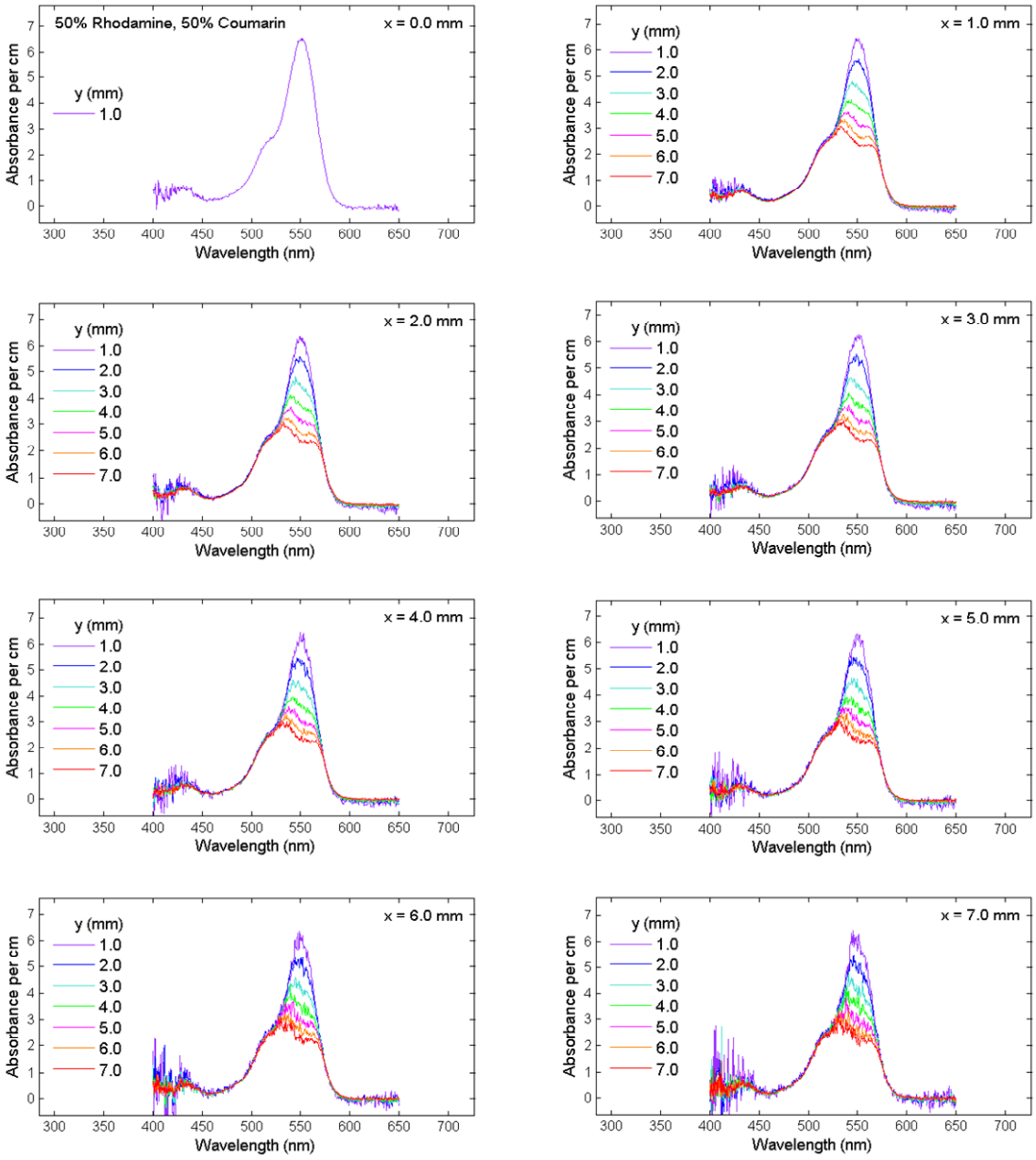

Fig. 16. Absorbance for a 50/50 mixture of the Coumarin and Rhodamine dyes calculated by applying Eq. (1) to the data displayed in Fig. 10.

4. Summary

This work has resulted in a data set rich in nonlinear effects to which we can apply multivariate approaches. With these data, we will assess the ability of principal component regression (PCR), partial least squares (PLS), classical least squares (CLS), and multivariate curve resolution (MCR) to understand linear and nonlinear effects when evaluating the fluorescence lidar signal return from optically thick media.

While the measurements described here were not subject to light scattering by the medium, scattering is also a critical issue associated with probing turbid samples (e.g., algae). Accounting for the effect of scattering to obtain "scattering-free" fluorescence spectra has been of interest to the research community for some time [27-35]. Light scattering could be incorporated into our experiment by adding a scattering matrix to the cuvette-contained samples. However, analyzing a particle size range of relevance to algal samples would require agitating the mixture to keep the particles from settling over the time span of the measurement. Such agitation can be readily provided by standard laboratory equipment (e.g., using small stir bars).

Finally, we note that while this project focused on interpreting data acquired through laser-based measurements, any mathematical approaches developed to account for nonlinear effects in these data would have applications well beyond lidar. In particular, the interpretation of multispectral/ hyperspectral data for classification or target detection is hindered by nonlinear effects such as Fresnel reflection, absorption, re-emission, scattering, and diffraction [36]. As with laser-induced fluorescence, forward models can be used to predict these effects [37], but improving solutions of the inverse problem is of high value. If multivariate approaches could account for nonlinear effects in a rigorous manner, this added capability would likely find broad use in the sensing community.

References

1. A. Hansch, D. Sauner, I. Hilger, J. Böttcher, A. Malich, O. Frey, R. Bräuer, W. A. Kaiser, Academic Radiology **11**, 1229-1236 (2004).
2. E. Sikorska, T. Gorecki, I. V. Khmelinskii, D. Sikorski, D. De Keukeleier, Food Chemistry **96**, 632-639 (2006).
3. R. D. JiJi, G. G. Andersson, and K. S. Booksh, "Application of PARAFAC for calibration with excitation-emission matrix fluorescence spectra of three classes of environmental pollutants," J. Chemometrics **14**, 171-185 (2000).
4. A. Manninen, M. Putkiranta, J. Saarela, A. Rostedt, T. Sorvajärvi, J. Toivonen, M. Marjamäki, J. Keskinen, and R. Hernberg, "Fluorescence cross sections of bioaerosols and suspended biological agents," Appl. Opt. **48**, 4320-4328 (2009).
5. O. Divya and A. K. Mishra, "Chemometric study of excitation-emission matrix fluorescence data: Quantitative analysis of petrol-kerosene mixtures," Appl. Spectrosc. **62**, 753-758 (2008).
6. J. A. Timlin, H. D. T. Jones, T. A. Reichardt, J. B. Ricken, J. Murton, B. Dwyer, A. Ruffing, A. August, S. C. James, S. Scholle, A. J. Powell, T. Turner, and D. T. Hansen, "Optimizing Algal Culture & Productivity: An Innovative, Multidiscipline, and Multiscale Approach," Presented at the Southwestern Biofuels Summit, Albuquerque, NM, April 13-14, 2010.
7. X. Luciana, S. Mounier, R. Redon, and A. Bois, "A simple correction method of inner filter effects affecting FEEM and its application to the PARAFAC decomposition," Chemom. Intell. Lab. Syst. **96**, 227-238 (2009).
8. B. Valeur, Molecular Fluorescence. Principles and Applications. Wiley-VCH, Weinheim (2002).
9. K. Adamsons, A. Timnick, J. F. Holland, and J. E. Sell, "Cell rotation for computer-based correction of primary and secondary absorption in fluorescence measurements," Anal. Chem. **54**, 2188-2190 (1982).
10. S. B. Sen-Gupta, J. Indian. Chem. Soc. **15**, 263-273 (1938).
11. H. Braunsberg and S. B. Osborn, "Some general aspects of fluorimetric determinations," Anal. Chim. Acta **6**, 84-95 (1952).
12. J. L. Lauer, "Correction for light absorption in fluorescence and light scattering measurements," J. Opt. Soc. Am. **41**, 482-483 (1951).
13. J. F. Thomas, M. Mukal, and D. B. Tebbens, "A geometrical aspect of fluorescent spectroscopy," Natl. Cancer Inst. Monogr. **9**, 127-133 (1962).
14. J. E. Gill, "Measurement of relative quantum yields of strongly absorbing solutions," Appl. Spectrosc. **24**, 588-590 (1970).
15. R. Van Slageren, G. Den Boef, and W. E. Van Der Linden, "The signal vs. concentration relationships in fluorimetry," Talanta **20**, 501-512 (1973).
16. J. F. Holland, R. E. Teets, and A. Timnick, "A unique computer centered instrument for simultaneous absorbance and fluorescence measurements," Anal. Chem. **45**, 145-153 (1973).
17. J. F. Holland, R. E. Teets, P. M. Kelly, and A. Timnick, "Correction of right-angle fluorescence measurements for the absorption of excitation radiation," Anal. Chem. **49**, 706-710 (1977).

18. A. Novak, “A method for routine corrections of inner filter effects in measurements of excitation and fluorescence spectra,” Collect. Czech. Chem. Commun. **43**, 2869-2878 (1978).

19. K. Adamsons, J. E. Sell, J. F. Holland, and A. Timnick, “Cell rotation method for absorption corrected measurements in molecular fluorescence,” American Laboratory **16**, 16-29 (1984)

20. D. R. Christmann, S. R. Crouch, J. F. Holland, and A. Timnick, “Correction of right-angle molecular fluorescence measurements for absorption of fluorescence radiation,” Anal. Chem. **52**, 291-295 (1980).

21. D. R. Christmann, S. R. Crouch, and A. Timnick, “Automated instrument for absorption-corrected molecular fluorescence measurements by the cell shift method,” Anal. Chem. **53**, 276-280 (1981).

22. D. R. Christmann, S. R. Crouch, and A. Timnick, “Precision and accuracy of absorption-corrected molecular fluorescence measurements by the cell shift method,” Anal. Chem. **53**, 2040-2044 (1981).

23. S. A. Tucker, V. L. Amszi, and W. E. Acree, Jr., “Primary and secondary inner filtering,” J. Chem. Edu. **69**, A8-A12 (1992).

24. T. Larsson, M. Wedborg, and D. Turner, “Correction of inner-filter effect in fluorescence excitation-emission matrix spectrometry using Raman scatter,” Anal. Chim. Acta **583**, 357-363 (2007).

25. K. W. Aniolek, R. L. Schmitt, T. J. Kulp, B. A. Richman, S. E. Bisson, and P. E. Powers, “Microlaser-pumped periodically poled lithium niobate optical parametric generator – optical parametric amplifer,” Opt. Lett. **25**, 557-559 (2000).

26. T. A. Reichardt, R. P. Bambha, T. J. Kulp, and R. L. Schmitt, “Frequency-locked, injection-seeded, pulsed narrowband optical parametric generator,” Appl. Opt. **42**, 3564-3569, (2003).

27. J. Wu, M. S. Field, and R. P. Rava, “Analytical model for extracting intrinsic fluorescence in turbid media,” Appl. Opt. **32**, 3585-3595 (1993).

28. A. J. Durkin, S. Jaikumar, N. Ramanujam, and R. Richards-Kortun, “Relation between fluorescence spectra of dilute and turbid samples,” Appl. Opt. **33**, 414-423 (1994).

29. S. A. Ahmed, Z.-W. Zang, K. M. Yoo, M. A. Ali, and R. R. Alfano, “Effect of multiple light scattering and self-absorption on the fluorescence and excitation spectra of dyes in random media,” Appl. Opt. **33**, 2748-2750 (1994).

30. C. M. Gardner, S. L. Jacques, and A. J. Welch, “Fluorescence spectroscopy of tissue: recovery of intrinsic fluorescence from measured fluorescence,” Appl. Opt. **35**, 1780-1792 (1996).

31. N. N. Zhadin and R. R. Alfano, “Correction of the internal absorption effect in fluorescence emission and excitation spectra from absorbing and highly scattering media: Theory and experiment,” J. Biomed. Opt. **3**, 171-186 (1998).

32. Q. Zhang, M. G. Müller, J. Wu, and M. S. Field, “Turbidity-free fluorescence spectroscopy of biological tissue,” Opt. Lett. **25**, 1451-1453 (2000).

33. M. G. Müller, I. Georgakoudi, Q. Zhang, J. Wu, and M. S. Field, “Intrinsic fluorescence spectroscopy in turbid media: disentangling effects of scattering and absorption,” Appl. Opt. **40**, 4633-4646 (2001).

34. R. Weersink, M. S. Patterson, K. Diamond, S. Silver, and N. Padgett, “Noninvasive measurement of fluorophore concentration in turbid media with a simple fluorescence/reflectance ratio technique,” Appl. Opt. **40**, 6389-6395 (2001).

35. N. C. Biswal, S. Gupta, N. Ghosh, and A. Pradhan, “Recovery of turbidity free fluorescence from measured fluorescence: an experimental approach,” Opt. Express **11**, 3320-3331 (2003).

36. N. Kesheva and J. F. Mustard, “Spectral unmixing,” IEEE Signal Process. Magazine, January 2002.

37. The Digital Imaging and Remote Sensing Image Generation Model (http://dirsig.org/).

Distribution:

1	MS9056	Thomas A. Reichardt (electronic copy)
1	MS1423	Randal L. Schmitt (electronic copy)
1	MS1423	Shane Sickafoose (electronic copy)
1	MS0895	Howland D. T. Jones (electronic copy)
1	MS0895	Jerilyn A. Timlin (electronic copy)
1	MS9056	Wen L. Hsu (electronic copy)
1	MS1423	Gregory A. Hebner (electronic copy)
1	MS0895	Anthony Martino (electronic copy)
1	MS9004	Duane Lindner (electronic copy)
1	MS0899	Technical Library, 9536 (electronic copy)